PHYSICAL REVIEW E **92**, 041101(R) (2015)

Coupled hydrodynamic model for laser-plasma interaction and hot electron generation

A. Colaïtis,[1] G. Duchateau,[1] X. Ribeyre,[1] Y. Maheut,[1] G. Boutoux,[1] L. Antonelli,[2,3] Ph. Nicolaï,[1] D. Batani,[1] and V. Tikhonchuk[1]

[1]*Université de Bordeaux–CNRS–CEA, Centre Lasers Intenses et Applications, UMR 5107, 351 Cours de la Libération, 33400 Talence, France*

[2]*Dipartimento SBAI, Università degli Studi di Roma "La Sapienza," Via Antonio Scarpa, 14, 00161 Rome, Italy*

[3]*Università di Roma "Tor Vergata," Dipartimento di Ingegneria Industriale, Via del Politecnico 1, 00133 Rome, Italy*

(Received 8 June 2015; published 29 October 2015)

We present a formulation of the model of laser-plasma interaction (LPI) at hydrodynamical scales that couples the plasma dynamics with linear and nonlinear LPI processes, including the creation and propagation of high-energy electrons excited by parametric instabilities and collective effects. This formulation accounts for laser beam refraction and diffraction, energy absorption due to collisional and resonant processes, and hot electron generation due to the stimulated Raman scattering, two-plasmon decay, and resonant absorption processes. Hot electron (HE) transport and absorption are described within the multigroup angular scattering approximation, adapted for transversally Gaussian electron beams. This multiscale inline LPI-HE model is used to interpret several shock ignition experiments, highlighting the importance of target preheating by HEs and the shortcomings of standard geometrical optics when modeling the propagation and absorption of intense laser pulses. It is found that HEs from parametric instabilities significantly increase the shock pressure and velocity in the target, while decreasing its strength and the overall ablation pressure.

DOI: 10.1103/PhysRevE.92.041101 PACS number(s): 52.25.Os, 52.35.Mw, 52.65.Kj

Laser-plasma interactions (LPIs) involving pulses of the order of [0.1,10] ns in the interaction regime $I\lambda^2 \in [10^{13}; 10^{16}]$ W μm^2/cm^2 are prone to various wave-plasma coupling processes [1]. Theoretical and experimental studies have shown that nonlinear LPIs play an important role in such configurations, notably relevant to high-energy density physics experiments involving laser beams and especially to inertial confinement fusion (ICF) [2]. Although these nonlinear LPIs are routinely studied at microscopic and mesoscopic scales using particle-in-cell (PIC) and paraxial electromagnetic codes, large scale models such as magnetohydrodynamic or radiative hydrodynamic codes are mostly limited to collisional absorption modeling. Inaccuracies in the description of linear and nonlinear LPIs at those scales are usually addressed by using time-varying limitations of the maximum electron thermal flux or adjusting the power distribution of laser beams to reproduce the experimental results. Such approaches hinder the understanding of the physical processes at play and limit the predictive capability of these tools. From these assessments, recent efforts have been made in describing nonlinear LPIs at hydrodynamical scales, notably in the case of inline solvers for cross-beam energy transfer [3–5] which have allowed one to better interpret and design ICF experiments and can be applied to assess novel laser configurations. Similarly, the effects of high-energy electron populations generated by nonlinear LPIs on the plasma dynamics are of particular importance for ICF studies [6,7], double ablation front experiments at high intensities, or for the design and interpretation of ns-scale laser target experiments in general [8]. Considering the large variety of laser-target configurations involving hot electron acceleration processes, there is an evident need for a multiscale model that can simultaneously account for, in hydrodynamic codes, linear and nonlinear LPIs, as well as the interwoven couplings between the laser propagation in plasmas, hot electron (HE) sources created by nonlinear LPIs, HE beam propagation, and plasma dynamics.

Modeling nonlinear LPIs and the laser-plasma-electron coupling on hydrodynamic scales poses severe difficulties related to the accurate description of the laser intensity in plasmas and the consistent description of HE sources from the laser propagation model. These limitations are related to the use of geometrical optics, which implies a needlelike ray description of the wave field as an almost-plane homogeneous wave [9], and does not allow for robust evaluations of the laser intensity in plasma [10]. Note that HE transport models with *ad hoc* sources are often included in such codes, usually using Monte Carlo approaches.

This Rapid Communication introduces an approach to hydrodynamic modeling that relies on paraxial complex geometrical optics (PCGO) [9,10] to describe the laser propagation in plasma using stochastically distributed Gaussian optical beamlets. It is coupled to a reduced HE transport model based on the angular scattering approximation (ASA) [11], adapted to two-dimensional (2D), transversally Gaussian, multigroup HE beams of arbitrary angular distribution, that computes their propagation and energy deposition. Considering the simultaneous and concurrent acceleration of hot electrons by resonant absorption (RA), stimulated Raman scattering (SRS), and two-plasmon decay (TPD), we present three simplified models for computing forward HE fluxes and temperatures from the optical beamlets of PCGO. This coupled LPI-HE model has been implemented in the CHIC arbitrary Lagrangian-Eulerian radiative hydrodynamic code [12], and is resolved inline, i.e., within hydrodynamic time steps. It is compared to the experimental results of laser absorption conducted at the Omega laser facility [13] and used to interpret the physical processes at play in a planar shock timing experiment in the framework of shock ignition ICF, in the Prague Asterix Laser System (PALS) [14]. An additional comparison is conducted to the experimental results of HE-assisted shock generation in a spherical configuration at Omega [15].

First, we introduce the reduced HE transport model developed for this study. The ASA model is derived from

the kinetic Vlasov-Fokker-Planck equation by considering electron-ion and electron-electron collisions. The HE distribution function is decomposed on the basis of spherical harmonics at first order, and the mean scattering angle $\langle\cos\theta\rangle(s) = \exp(-\int_0^s k_1(s')ds')$ is expressed as a function of the curvilinear electron beam coordinate s. The transport cross section k_1 includes the differential angular deviation, and accounts for Debye screening, quantum effects [11,16,17], and nonideal plasma conditions [18]. Assuming the HE beam propagates along a straight line, the energy loss reads $d\epsilon/ds = -S(\epsilon)/\langle\cos\theta\rangle(s)$, where S is the electron stopping power [19] that is induced by bound electrons, free electrons, and plasmons [11,17,18]. The angular scattering on background electrons and ions widens the beam as $d\Delta/ds = 2\langle\tan\theta\rangle(s)$, a significant process in ICF conditions [11]. Each HE beam is described by an exponential distribution function in energy $f_E(\epsilon) \propto \exp(-\epsilon/T_\mathrm{h})$ that is logarithmically discretized in a series of monoenergetic beamlets.

This multigroup model for HE beam transport in plasmas has been validated with a reference code [20] for various cases in homogeneous and inhomogeneous plasmas using 50 groups in energy, ranging from $T_\mathrm{h}/5$ to $8T_\mathrm{h}$, for various angles of incidence and initial beam apertures. The free parameters defining a given HE source are the initial energy flux F_e, mean temperature T_h, angular distribution, and direction. Those parameters are determined from both laser and plasma characteristics, thus coupling nonlinear LPIs to HE sources.

We first consider the case of HE beams created by resonant laser absorption. For a p-polarized electromagnetic wave incident at an angle φ (defined at the plasma-vacuum boundary) on a linear density profile of scale length L, the fraction of beam energy f_A absorbed at the critical density can be expressed as $f_A = \Phi^2(\eta_c)/2$ [21], with $\eta_c = (\omega L/c)^{2/3}\sin^2\varphi$ and Φ a resonance function. Based on Ref. [22], we have derived a resonance function where the decay factor of the electric field is estimated without the Wentzel-Kramers-Brillouin (WKB) approximation, $\Phi(\eta_c) \simeq 1.866\eta_c^{1/2}\exp(-2\eta_c^{3/2}/3)/(\eta_c + 0.435)^{1/4}$. Compared to numerical solutions of the wave equation and PIC simulations [23], this formulation captures the absorption fraction to within an error of 10%, and yields an optimal angle of $\eta_c = 0.51$ that is bracketed by the simulation values ($\eta_c \in [0.47; 0.53]$). When a p-polarized PCGO beamlet propagates orthogonally to the density gradient direction, a HE beam is initialized at the critical density, parallel to the gradient direction. For the resonant absorption and any LPI-HE source presented here, the power fraction transferred to the electron source is removed from the PCGO beamlet at its turning point. Simultaneously, the intensity, curvature radius, and width of the optical beamlet is recomputed downstream of the LPI location, in order to consistently model further interactions of the beamlet with the plasma. Additionally, the transverse width of the HE source is taken to be that of the optical beamlet. The HE mean energy for the resonant absorption is computed using scaling laws from several experimental campaigns, conducted for various interaction parameters and wavelengths [24,25],

$$\begin{aligned} T_\mathrm{h}^\mathrm{RA} &= 9.37\times10^{-10}(I\lambda^2)^{0.664}\ \mathrm{keV}, \quad I\lambda^2 \in [10^{13};10^{15}],\\ T_\mathrm{h}^\mathrm{RA} &= 1.58\times10^{-3}(I\lambda^2)^{0.247}\ \mathrm{keV}, \quad I\lambda^2 \in [10^{15};10^{17}], \end{aligned} \tag{1}$$

where the beamlet intensity I is in units of W/cm^2 and λ in μm.

The characterization of HE sources from parametric instabilities is inherently more challenging. Theoretical works have demonstrated that the temperature of TPD-HEs is not related to the electron plasma wave's (EPW's) phase velocity at the quarter critical density, because electrons undergo a stage acceleration [26]. Time-dependent scaling laws for F_e^TPD and $T_\mathrm{h}^\mathrm{TPD}$ as a function of laser intensity were proposed in Ref. [27], from extensive PIC simulations in the 10^{15}–10^{16} W/cm^2 intensity range with $\lambda = 351$ nm and in plasmas of electron temperature $T_e \approx 2$ keV. The steady-state values of these scaling laws are used to define HE sources from TPD,

$$\begin{aligned} F_e^\mathrm{TPD} &= 2.6\times10^{-2} I\{1-\exp[-(\xi^\mathrm{TPD}-1)^{1/2}]\}\ \mathrm{W/cm^2},\\ T_\mathrm{h}^\mathrm{TPD} &= 15.5 + 17.7\xi^\mathrm{TPD}\ \mathrm{keV}, \end{aligned} \tag{2}$$

where $\xi^\mathrm{TPD} = I/I_\mathrm{th}^\mathrm{TPD}$ is the relative intensity of the drive, and $I_\mathrm{th}^\mathrm{TPD}$ the threshold intensity for TPD in an inhomogeneous plasma, $I_\mathrm{th}^\mathrm{TPD} = 8.2T_\mathrm{keV}/(L_{\mu\mathrm{m}}\lambda_{\mu\mathrm{m}})$ PW/cm^2 [22,28], with $L_{\mu\mathrm{m}}$ being the local density scale length in μm. The EPWs excited by TPD have privileged directions at $\pm45^\circ$ with respect to the pump. Shared pump wave processes and plasma density modulations have been shown to be significant in ICF regimes [29,30], and spread the optimal angle of forward HE emission in various directions in that cone. We assume that the multiplicity of configurations for the pump and daughter waves produces a uniform HE emission in the -45° to $+45^\circ$ cone with respect to the PCGO ray direction. This spread is obtained by superimposing electron beamlets at various angles. HEs from TPD are emitted at $n_c/4$, both forward and backward.

Contrary to the TPD process, the energy of SRS-induced HE is correlated with the phase velocity of the EPW at its point of resonance and not with the drive intensity ξ^SRS [31]. Conversely, the number of HEs is seen to scale with ξ^SRS. The asymptotic HE flux is set to 12.5% of the pump intensity, which is the maximum number of forward HEs that SRS can drive in a steady state [32]. The shape of the flux function F_e is chosen to be similar to that of TPD, and rearranged to correspond to experimental estimates [8,15],

$$F_e^\mathrm{SRS} = 12.5\times10^{-2} I\{1-\exp[-(\xi^{1/3}-1)]\}\ \mathrm{W/cm^2}. \tag{3}$$

The relative intensity ξ^SRS is defined with respect to the absolute instability threshold in an inhomogeneous plasma and at the quarter critical density, $I_\mathrm{th}^\mathrm{SRS} = 99.5/(L_{\mu\mathrm{m}}^2\lambda_{\mu\mathrm{m}})^{2/3}$ PW/cm^2 [33,34]. In order to account for the Raman gap observed in experiments [1,35], we assume SRS takes place at $n_e = 0.2n_c$. Under those assumptions, the HE temperature reads

$$T_\mathrm{h}^\mathrm{SRS} = \frac{m_e v_\mathrm{ph}^2}{2}, \quad v_\mathrm{ph} = \frac{v_\mathrm{te}\sqrt{1+3(k_\mathrm{pe}\lambda_D)^2}}{k_\mathrm{pe}\lambda_D}, \tag{4}$$

where v_ph is the EPW phase velocity, λ_D the Debye length, k_pe the EPW wave number, and v_te the electron thermal velocity. Experiments have shown that SRS-driven HEs are directional with respect to the laser drive [36]. Consequently, HE sources from SRS are initialized in the direction of the pump wave with no initial angular spread.

This model has been tested in the case of laser absorption in plasmas, by comparison to an experiment conducted at the Omega laser facility [37], where a 940 μm diameter spherical plastic target is irradiated by 60 s- and p-polarized beams in two picket pulses ($\sim$100 ps) of 12 and 18 J per beam, respectively (peak intensity $\approx 5 \times 10^{14}$ W/cm^2). Contrary to hydrodynamic computations presented in Ref. [37], the LPI-HE model is able to reproduce the correct laser absorption in both picket pulses simultaneously, using a fixed value of the electron flux limiter $f_L = 0.04$ [38] instead of a time-varying one. This improvement lies in (i) the description of resonant absorption, that is prominent here, and (ii) the correct description of the wave field close to the critical density as an almost-plane inhomogeneous wave in PCGO, contrary to GO for which the slowly varying envelope approximation is no longer valid.

Laser-plasma configurations prone to parametric instabilities are now considered. Experimental studies of HE coupling to plasmas in ICF regimes were performed on the PALS laser system in Prague [8]. The experimental setup involves a sequence of two laser pulses of 300 ps full width at half maximum (FWHM) duration: a preheating low intensity beam at 1ω ($\lambda = 1315$ nm, $\theta = 30^\circ$, $I \simeq 10^{14}$ W/cm^2) and a normally incident high intensity beam at 3ω ($I \simeq 5 \times 10^{15}$–$3 \times 10^{16}$ W/cm^2). The targets are composed of a 25 μm thick plastic ablator and various tracer layers: 25 μm Al (CHAl targets), 5 μm Cu and 20 μm Al (CHCuAl targets), and 10 μm Ti and 10 μm Cu (CHTiCu targets). The plastic layer mimics the typical ablator used in ICF and the low intensity beam is used to create a coronal plasma. The shock produced by ablation of the plastic layer is studied using the shock breakout chronometry on the target's backside by streak optical pyrometry. The HE population is estimated by reproducing the measured $K\alpha$ emission with Monte Carlo (MC) simulations of electrons propagating in the stationary target [39], using the GEANT4 and PENELOPE codes [40,41]. For the CHTiCu target, the experimental data are reproduced with HE temperatures of 25.3 ± 7.6 keV and energy fluxes of $0.7 \pm 0.4\%$ of the incident laser energy. These are in good agreement with other data, e.g., Refs. [42] (PALS, $T_h \approx 50 \pm 10$ keV, CHCuAl targets), [43] (Omega, $T_h \approx 30$ keV), and [44] (PIC calculations, $T_h = 20$–40 keV).

Simulations of the experiments for three multilayered targets are conducted with the CHIC code using the multiscale LPI-HE model and compared to GO-based models, systematically using nominal experimental parameters: measured laser energy, focal spot and temporal pulse shape, and nominal target configuration. A comparison of experimental and simulation results for the shock chronometry is presented in Fig. 1. Simulations with GO predict a shock breakout time much shorter than the experimental timings by up to a factor of 2.5. Results from the LPI-HE model are significantly closer to experimental data for all intensities and targets, owing to the modified target dynamics from HE preheat that is accounted for and to more precise collisional absorption modeling. We discuss the physical processes at play by detailing the case of the CHTiCu targets.

Early in the interaction, 1.3% of the laser energy is resonantly absorbed at the critical surface layer, thus increasing the shock pressure and velocity, and reducing the shock

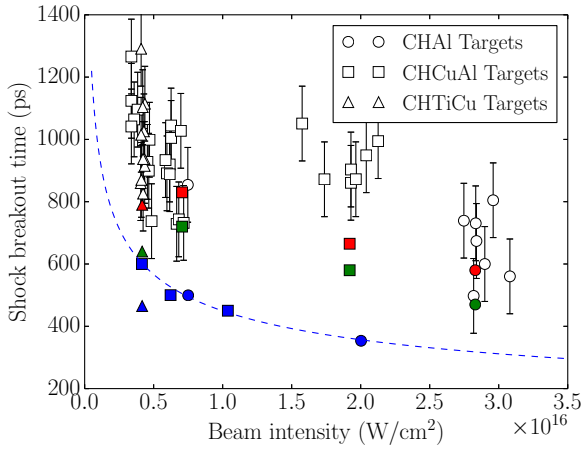

FIG. 1. (Color online) Shock breakout time vs laser intensity for various targets. Open symbols are experimental points. Colored symbols are from hydrodynamic simulations, with GO in blue (dark gray), the present LPI-HE model in red (light gray), and PCGO only in green (gray). The standard $P_{choc} \propto I^{2/3}$ and $v_{choc} \propto P^{1/2}$ scaling is shown as dashed blue (dark gray) lines.

breakout time by 30 ps. Starting slightly later, SRS and TPD-generated HE beams gradually preheat the bulk of the target both in front and behind of the shock to a few tens of eV, as illustrated in Fig. 2. Averaged temperatures and fluxes for these HE beams are of 40.7 keV and 1.17% of the laser energy, respectively. These values are slightly above the MC estimate, although the tracers in the target may not be sensitive enough to electron populations of higher energies. Preheating of the dense cold target raises the plasma pressure at a nearly constant density, thus increasing the shock velocity (function of $\sqrt{P/\rho}$). The HE preheat also raises the local sound velocity, thus decreasing the strength of the shock, by up to a factor of 2.78 during the laser drive. Although the shock strength is lower, the local pressure increase leads to a postshock pressure that is higher with HEs, up to +40% with respect to simulations without HEs, depending on the targets. The effects of HEs on the overall ablation pressure is difficult to

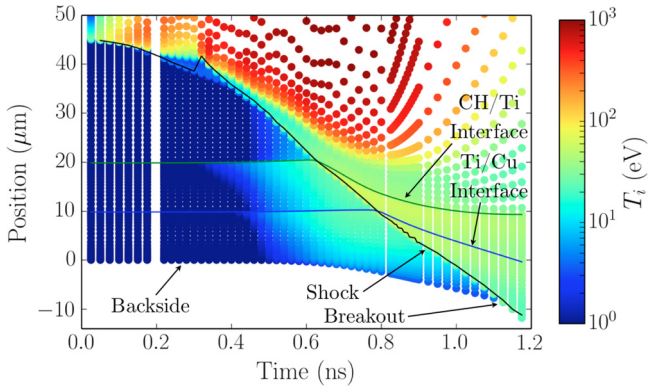

FIG. 2. (Color online) Log-scaled ion temperature (eV) of the CHTiCu target as a function of time (ns) and depth in the target (μm), along the laser axis. The solid lines show the locations of the tracer interfaces.

estimate in this experiment because of the interference of tracer materials in the overall plasma dynamics. Simultaneously to the bulk preheat, LPI-generated HEs that reach the target's rear surface heat it to several eV, thus initiating a backside plasma expansion that delays the shock breakout (see the rear target interface in Fig. 2). For that reason, simulations with PCGO and without HE fortuitously reproduce similar shock timings: The lower shock velocity is compensated by the absence of backside target expansion. The integrated reflectivity in the simulation is 28%, in good agreement with the experimental measurements of $25 \pm 10\%$.

The multiscale LPI-HE model is now applied to a recent experiment on Omega [15,45] that illustrated the importance of LPI-generated HEs on shock dynamics. A spherical 430 μm diameter target of Ti-doped plastic with a plastic ablator is irradiated by a shaped pulse of peak intensity $\sim 5 \times 10^{15}$ W/cm^2. The shock is observed to reach the target center at $t_c = 1.98$ ns, for an integrated laser absorption of $\mathcal{F}_{\text{exp}} = 55 \pm 5\%$ and HE energy fraction of $\sim 8\%$ in the 50–100 keV range. A 2D axisymmetric simulation using the LPI-HE model with the target and impulsion data yields $t_c = 1.976$ ns, with 7.3% of laser energy converted into forward HEs at an average suprathermal temperature of 83 keV for the TPD-HEs, 41 keV for the SRS-HEs, and an additional 1.2% of HEs produced by RA at 1.6 keV. The overall laser absorption in the simulation is of $\mathcal{F}_{\text{HE}} = 51.7\%$, with 42% of collisional absorption. Shock timing, overall absorption, laser to HE conversion, and HE temperatures simultaneous match the experimental data within the error bars. We note that the levels of SBS in both experiments are such that simulation results remain within the experimental error bars. Results are compared to a simulation without HEs, adjusted so that absorption matches the experimental data with $\mathcal{F}_{\text{noHE}} = 57\%$. Similar to the PALS campaign results, it is found that HEs decrease the shock strength (by $\sim 20\%$) while the pressure behind of the shock increases (by $\sim 20\%$). The shock timing with HEs is reduced by 100 ps, a signature of a faster shock due to plasma bulk preheating. Additionally, it is found that the maximum ablation pressure is decreased by 30%, as LPI-generated HEs deposit their energy beyond the ablation front and thus weakly contribute to it, while the collisional absorption is overall lower when considering nonlinear LPIs.

Results using our LPI-HE model exhibit a significant improvement in hydrodynamic modeling, simultaneously matching data from hydrodynamics, hot electrons, and reflectivity measurements with HE parameters being computed inline from the LPI. The theoretical and experimental laws used for the LPI-HE coupling have been validated against experimental data obtained in planar and spherical laser-target geometries, for pulse lengths in the $[0.1; 2]$ ns regime and interaction parameters in the $[10^{13}; 4 \times 10^{15}]$ W μm^2/cm^2 range, and is expected to hold for pulses of the order of 10 ns and up to 1×10^{16} W μm^2/cm^2. The LPI-HE model allows to constrain simultaneously the global laser absorption, the hydrodynamics of the target, and the HE preheat. Application of this coupled model has shown that LPI-generated HEs significantly decrease the shock strength and the ablation pressure for interactions in plastic targets. While it was found that the postshock pressure is enhanced with HEs, the deep target preheat observed in the experiment may be detrimental for fusion applications. This formulation is readily applicable to direct-drive ICF as well as to the interpretation of laser-target experiments in high-energy density physics. Particularly, it is expected to provide insight into the physics of shock ignition ICF. Although the stimulated Brillouin scattering and stimulated electron acoustic scattering remain to be described in this approach, the formalism presented here is compatible with their implementation. Similarly, the framework presented here is compatible with refinements of the LPI models in order to account for finer kinetic effects.

This work has been carried out within the framework of the EUROfusion consortium and has received funding from the European Union's Horizon 2020 research and innovation programme under Grant Agreement No. 633053. This work is partially supported by the COST action MP1208 and the project ANR-12-BS04-0006-04 from the French National Research Agency. The authors wish to thank R. Nora and W. Theobald for having made available the spherical strong-shock data presented in this Rapid Communication (shot No. 71597).

[1] K. Tanaka, L. M. Goldman, W. Seka, M. C. Richardson, J. M. Soures, and E. A. Williams, Phys. Rev. Lett. **48**, 1179 (1982).

[2] S. Atzeni and J. Meyer-ter Vehn, *The Physics of Inertial Fusion*, International Series of Monographs on Physics (Oxford University Press, Oxford, UK, 2004).

[3] P. Michel, L. Divol, E. A. Williams, S. Weber, C. A. Thomas, D. A. Callahan, S. W. Haan, J. D. Salmonson, S. Dixit, D. E. Hinkel, M. J. Edwards, B. J. MacGowan, J. D. Lindl, S. H. Glenzer, and L. J. Suter, Phys. Rev. Lett. **102**, 025004 (2009).

[4] I. V. Igumenshchev, D. H. Edgell, V. N. Goncharov, J. A. Delettrez, A. V. Maximov, J. F. Myatt, W. Seka, A. Shvydky, S. Skupsky, and C. Stoeckl, Phys. Plasmas **17**, 122708 (2010).

[5] A. Colaïtis, G. Duchateau, X. Ribeyre, and V. Tikhonchuk, Phys. Rev. E **91**, 013102 (2015).

[6] R. Betti, C. D. Zhou, K. S. Anderson, J. L. Perkins, W. Theobald, and A. A. Solodov, Phys. Rev. Lett. **98**, 155001 (2007).

[7] D. Batani, S. Baton, A. Casner, S. Depierreux, M. Hohenberger, O. Klimo, M. Koenig, C. Labaune, X. Ribeyre, C. Rousseaux, G. Schurtz, W. Theobald, and V. Tikhonchuk, Nucl. Fusion **54**, 054009 (2014).

[8] D. Batani, L. Antonelli, S. Atzeni, L. Antonelli, S. Atzeni, J. Badziak, F. Baffigi, T. Chodukowski, F. Consoli, G. Cristoforetti, R. D. Angelis, R. Dudzak, G. Folpini, L. Giuffrida, L. A. Gizzi, Z. Kalinowska, P. Koester, E. Krousky, M. Krus, L. Labate, T. Levato, Y. Maheut, G. Malka, D. Margarone, A. Marocchino, J. Nejdl, P. Nicolai, T. O'Dell, T. Pisarczyk, O. Renner, Y. J. Rhee, X. Ribeyre, M. Richetta, M. Rosinski, M. Sawicka, A. Schiavi, J. Skala, M. Smid, C. Spindloe, J. Ullschmied, A. Velyhan, and T. Vinci, Phys. Plasmas **21**, 032710 (2014).

[9] Y. A. Kravtsov and N. Y. Zhu, *Theory of Diffraction, Heuristic Approaches*, Alpha Science Series on Wave Phenomena (Alpha Science International, Oxford, UK, 2010).

[10] A. Colaïtis, G. Duchateau, P. Nicolaï, and V. Tikhonchuk, Phys. Rev. E **89**, 033101 (2014).

[11] C. K. Li and R. D. Petrasso, Phys. Rev. E **70**, 067401 (2004).

[12] J. Breil, S. Galera, and P. H. Maire, Comput. Fluids **46**, 161 (2011).
[13] T. Boehly, D. Brown, R. Craxton, R. Keck, J. Knauer, J. Kelly, T. Kessler, S. Kumpan, S. Loucks, S. Letzring, F. Marshall, R. McCrory, S. Morse, W. Seka, J. Soures, and C. Verdon, Opt. Commun. **133**, 495 (1997).
[14] K. Jungwirth, A. Cejnarova, L. Juha, B. Kralikova, J. Krasa, E. Krousky, P. Krupickova, L. Laska, K. Masek, T. Mocek, M. Pfeifer, A. Präg, O. Renner, K. Rohlena, B. Rus, J. Skala, P. Straka, and J. Ullschmied, Phys. Plasmas **8**, 2495 (2001).
[15] R. Nora, W. Theobald, R. Betti, F. J. Marshall, D. T. Michel, W. Seka, B. Yaakobi, M. Lafon, C. Stoeckl, J. Delettrez, A. A. Solodov, A. Casner, C. Reverdin, X. Ribeyre, A. Vallet, J. Peebles, F. N. Beg, and M. S. Wei, Phys. Rev. Lett. **114**, 045001 (2015).
[16] C. K. Li and R. D. Petrasso, Phys. Rev. E **73**, 016402 (2006).
[17] A. A. Solodov and R. Betti, Phys. Plasmas **15**, 042707 (2008).
[18] L. Gremillet, Theoretical and experimental study of fast electron transport in ultra-high-intensity laser-solid interaction french PhD Thesis, Ecole Polytechnique, Palaiseau, 2003.
[19] H. A. Bethe, *Handbuch für Physik* (Springer, Berlin, 1933), Vol. 24/2, p. 273.
[20] M. Touati, J.-L. Feugeas, P. Nicolaï, J. J. Santos, L. Gremillet, and V. T. Tikhonchuk, New J. Phys. **16**, 073014 (2014).
[21] V. L. Ginzburg, *The Properties of Electromagnetic Waves in Plasma* (Pergamon, New York, 1964).
[22] W. L. Kruer, *The Physics of Laser Plasma Interactions* (Westview Press, University of California, Los Angeles, 2003).
[23] D. W. Forslund, J. M. Kindel, K. Lee, E. L. Lindman, and R. L. Morse, Phys. Rev. A **11**, 679 (1975).
[24] F. Amiranoff, R. Fabbro, E. Fabre, C. Garban-Labaune, and M. Weinfeld, J. Phys. (France) **43**, 1037 (1982).
[25] D. C. Slater, G. E. Busch, G. Charatis, R. R. Johnson, F. J. Mayer, R. J. Schroeder, J. D. Simpson, D. Sullivan, J. A. Tarvin, and C. E. Thomas, Phys. Rev. Lett. **46**, 1199 (1981).
[26] R. Yan, C. Ren, J. Li, A. V. Maximov, W. B. Mori, Z.-M. Sheng, and F. S. Tsung, Phys. Rev. Lett. **108**, 175002 (2012).
[27] H. X. Vu, D. F. DuBois, J. F. Myatt, and D. A. Russell, Phys. Plasmas **19**, 102703 (2012).
[28] B. B. Afeyan and E. A. Williams, Phys. Plasmas **4**, 3827 (1997).
[29] S. Weber, C. Riconda, O. Klimo, A. Héron, and V. T. Tikhonchuk, Phys. Rev. E **85**, 016403 (2012).
[30] J. F. Myatt, J. Zhang, R. W. Short, A. V. Maximov, W. Seka, D. H. Froula, D. H. Edgell, D. T. Michel, I. V. Igumenshchev, D. E. Hinkel, P. Michel, and J. D. Moody, Phys. Plasmas **21**, 055501 (2014).
[31] O. Klimo and V. T. Tikhonchuk, Plasma Phys. Controlled Fusion **55**, 095002 (2013).
[32] L. Yin, B. J. Albright, H. A. Rose, K. J. Bowers, B. Bergen, D. S. Montgomery, J. L. Kline, and J. C. Fernndez, Phys. Plasmas **16**, 113101 (2009).
[33] C. S. Liu, in *Advances in Plasma Physics*, edited by A. Simon and W. B. Thompson (Wiley, New York, 1976), pp. 121–177.
[34] B. B. Afeyan and E. A. Williams, Phys. Plasmas **4**, 3803 (1997).
[35] C. Labaune, H. A. Baldis, E. Fabre, F. Briand, D. M. Villeneuve, and K. Estabrook, Phys. Fluids B **2**, 166 (1990).
[36] C. Rousseaux, F. Amiranoff, C. Labaune, B. Mabille, and G. Matthieussent, Rev. Phys. Appl. (Paris) **23**, 1515 (1988).
[37] S. P. Regan, R. Epstein, V. N. Goncharov, I. V. Igumenshchev, D. Li, P. B. Radha, H. Sawada, W. Seka, T. R. Boehly, J. A. Delettrez, O. V. Gotchev, J. P. Knauer, J. A. Marozas, F. J. Marshall, R. L. McCrory, P. W. McKenty, D. D. Meyerhofer, T. C. Sangster, D. Shvarts, S. Skupsky, V. A. Smalyuk, B. Yaakobi, and R. C. Mancini, Phys. Plasmas **14**, 056305 (2007).
[38] A. R. Bell, R. G. Evans, and D. J. Nicholas, Phys. Rev. Lett. **46**, 243 (1981).
[39] K. B. Wharton, S. P. Hatchett, S. C. Wilks, M. H. Key, J. D. Moody, V. Yanovsky, A. A. Offenberger, B. A. Hammel, M. D. Perry, and C. Joshi, Phys. Rev. Lett. **81**, 822 (1998).
[40] J. Sempau, E. Acosta, J. Baro, J. Fernández-Varea, and F. Salvat, Nucl. Instrum. Methods Phys. Res., Sect. B **132**, 377 (1997).
[41] S. Agostinelli, J. Allison, K. Amako, J. Apostolakis, H. Araujo, P. Arce, M. Asai, D. Axen, S. Banerjee, G. Barrand, F. Behner, L. Bellagamba, J. Boudreau, L. Broglia, A. Brunengo, H. Burkhardt, S. Chauvie, J. Chuma, R. Chytracek, G. Cooperman, G. Cosmo, P. Degtyarenko, A. Dell'Acqua, G. Depaola, D. Dietrich, R. Enami, A. Feliciello, C. Ferguson, H. Fesefeldt, G. Folger, F. Foppiano, A. Forti, S. Garelli, S. Giani, R. Giannitrapani, D. Gibin, J. G. Cadenas, I. Gonzalez, G. G. Abril, G. Greeniaus, W. Greiner, V. Grichine, A. Grossheim, S. Guatelli, P. Gumplinger, R. Hamatsu, K. Hashimoto, H. Hasui, A. Heikkinen, A. Howard, V. Ivanchenko, A. Johnson, F. Jones, J. Kallenbach, N. Kanaya, M. Kawabata, Y. Kawabata, M. Kawaguti, S. Kelner, P. Kent, A. Kimura, T. Kodama, R. Kokoulin, M. Kossov, H. Kurashige, E. Lamanna, T. Lampén, V. Lara, V. Lefebure, F. Lei, M. Liendl, W. Lockman, F. Longo, S. Magni, M. Maire, E. Medernach, K. Minamimoto, P. M. de Freitas, Y. Morita, K. Murakami, M. Nagamatu, R. Nartallo, P. Nieminen, T. Nishimura, K. Ohtsubo, M. Okamura, S. O'Neale, Y. Oohata, K. Paech, J. Perl, A. Pfeiffer, M. Pia, F. Ranjard, A. Rybin, S. Sadilov, E. D. Salvo, G. Santin, T. Sasaki, N. Savvas, Y. Sawada, S. Scherer, S. Sei, V. Sirotenko, D. Smith, N. Starkov, H. Stoecker, J. Sulkimo, M. Takahata, S. Tanaka, E. Tcherniaev, E. S. Tehrani, M. Tropeano, P. Truscott, H. Uno, L. Urban, P. Urban, M. Verderi, A. Walkden, W. Wander, H. Weber, J. Wellisch, T. Wenaus, D. Williams, D. Wright, T. Yamada, H. Yoshida, and D. Zschiesche, Nucl. Instrum. Methods Phys. Res., Sect. A **506**, 250 (2003).
[42] L. Antonelli, M. Richetta, P. Koester, L. Labate, T. Levato, L. Gizzi, E. Krousky, J. Skala, R. Dubzak, J. Ullshimied, O. Renner, M. Smid, M. Rosinski, J. Badziak, T. Pisarczyk, Z. Kalinowska, and T. Chodukowski, in *Proceedings of 39th EPS Conference & 16th International Congress on Plasma Physics* (European Physical Society, Mulhouse, France, 2013), p. 461.
[43] W. Theobald, R. Nora, M. Lafon, A. Casner, X. Ribeyre, K. S. Anderson, R. Betti, J. A. Delettrez, J. A. Frenje, V. Y. Glebov, O. V. Gotchev, M. Hohenberger, S. X. Hu, F. J. Marshall, D. D. Meyerhofer, T. C. Sangster, G. Schurtz, W. Seka, V. A. Smalyuk, C. Stoeckl, and B. Yaakobi, Phys. Plasmas **19**, 102706 (2012).
[44] O. Klimo, S. Weber, V. T. Tikhonchuk, and J. Limpouch, Plasma Phys. Controlled Fusion **52**, 055013 (2010).
[45] W. Theobald, R. Nora, W. Seka, M. Lafon, K. S. Anderson, M. Hohenberger, F. J. Marshall, D. T. Michel, A. A. Solodov, C. Stoeckl, D. H. Edgell, B. Yaakobi, A. Casner, C. Reverdin, X. Ribeyre, A. Shvydky, A. Vallet, J. Peebles, F. N. Beg, M. S. Wei, and R. Betti, Phys. Plasmas **22**, 056310 (2015).